Chemical routes to materials

Enhanced photocatalytic performance of electrospun hollow titanium dioxide nanofibers decorated with graphene quantum dots

Peipei Huo[1,*] (ID), Peng Zhao[1,2], Xiaobo Shi[3], Ziyan Zhou[4], and Bo Liu[1,*] (ID)

[1] *Laboratory of Functional Molecules and Materials, School of Physics and Optoelectronic Engineering, Shandong University of Technology, Xincun West Road 266, Zibo 255000, China*

[2] *School of Materials Science and Engineering, Shandong University of Technology, Xincun West Road 266, Zibo 255000, China*

[3] *Institute of Artificial Intelligence, Henan Finance University, Zhengzhou 450046, China*

[4] *School of Chemistry and Chemical Engineering, Shandong University of Technology, Xincun West Road 266, Zibo 255000, China*

ABSTRACT

Titanium dioxide (TiO_2) is an outstanding photocatalytic semiconductor, but wide band gap of TiO_2 significantly restricts its photocatalytic performance. Graphene possesses promising mechanical, optical and electrical properties. Relying on the excellent gain effect of graphene quantum dots (GQDs) on conductivity, unique up-conversion photoluminescence property and remarkable dye adsorption, the photoelectric properties of TiO_2 can be significantly improved. In this study, a novel structure of GQDs-decorated TiO_2 nanofibers was successfully prepared by electrospinning and hydrothermal synthesis procedures. The synthesized GQDs/TiO_2 nanofibers composite exhibited a one-dimensional structure. The results show that introduction of GQDs prohibits the adverse recombination between photoinduced charges and prolongs the existence time. The photocatalytic properties characterization results show that 10% mass fraction of GQDs in composite nanofibers has the best degradation activity with its ultrafast electron transport rate and low electron–hole pair recombination rate.

Introduction

With the evolution of society and the development of science and technology, global environmental pollution has been kept increasing and has become a burning issue that needs urgent solution. Emission of hazardous chemicals in the procedure of using fossil fuels poses a huge burden to the clean-up of the environment [1, 2] and has become a major problem that restricts sustainable development. One among the most devastating problems our environment

---

Handling Editor: Annela M. Seddon.

Address correspondence to E-mail: peipeihuo@sdut.edu.cn; liub@sdut.edu.cn

faces is the large amount of sewage emission containing harmful substance. It costs a lot of manpower, material resources and financial resources on the cleaning of industrial waste water every year, and it also brings secondary pollution in the process of environmental management. Conventional processes involve unnecessary intermediate by-products that require complex post-treatment to resolve. In contrast, photocatalysis stands out as an effective way to use sustainable solar energy to decompose pollutants with environment friendly advantage. In recent years, semiconductors photocatalysis has been highly valued by the scientific community because of good photocatalytic efficiency, low price, high stability and extensive degradation. In semiconductors' photocatalytic scenario, solar energy can be absorbed and utilized by semiconductors owing to their distinguished electronic states. An irradiation light with a surplus energy compared with the band gap can excite electrons, therefore separating electron and holes. The photoinduced charge carriers can subsequently degrade organic pollutants.

Among those many semiconductors that are enabled to photodegrade environmental pollutants, titanium dioxide (TiO_2) is the mostly intensively investigated [3–6]. TiO_2 has generally excellent features including non-toxicity, chemical stability and photocatalytic properties to extensively degrade various organic pollutants. Therefore, TiO_2 catalyst has a wide application prospects in the fields such as environmental treatment and solar cells [7–9]. However, photocatalytic properties of TiO_2 is by a great deal limited by TiO_2's band gap (3.2 eV), resulting in light absorption limited to the ultraviolet region, thus leading to a relatively poor photocatalytic efficiency with visible light. Upon irradiation, photogenerated electron–hole pairs (EHPs) are formed and then organic matter is decomposed by strong oxidation of holes and active hydroxyl radicals. Nonetheless, the EHPs exhibit an enormously short life time before their recombination (10^{-9} s), which hampers the evolution of photocatalysis procedure. Therefore, poor solar light efficiency and high charge carrier recombination rate are two major disadvantages for TiO_2 photocatalysis [10–12].

There have been many approaches to modify the current photocatalysis; for example, a two-dimensional system could provide sufficient active sites and good transport properties [13], and a plasmonic photocatalyst could exhibit excellent visible-light

harvesting ability [14]. It is especially important to modify TiO_2 by some technical means to narrow down the band gap width, facilitate the electron transfer, or expand the light-responsive region. One promising solution which could solve the problem is to utilize various approaches such as metal or non-metal elements doping into TiO_2 [15–18] and use of quantum dots possessing small band gap [6, 19], which was reported to be able to span the UV plus visible segment in solar spectrum [19]. Graphene is a monolayer crystal of graphite with its carbon atoms arranging as honeycombed crystal lattices with sp^2 hybridization orbits [20]. As fragments of graphene, graphene quantum dots (GQDs) are 0-dimensional nanomaterials [21, 22]. Because the movement of electrons in all directions is limited by small size, the quantum confinement effect of GQDs is particularly remarkable [23, 24]. Besides high conductivity and photoluminescence (PL) effects, GQDs also have many novel chemical and physical properties such as highly accessible surface areas, high chemical stability, low cytotoxicity, very good biocompatibility and excellent water solubility. Thanks to these advantages, GQDs show great prospects in optoelectronic devices, detectors, bio-imaging, etc.[25].

There have been previous attempts of composing TiO_2 with GQDs materials. GQDs-decorated TiO_2 was prepared where the synergetic effect of GQDs led to enhancement in visible-light absorption and inhibition in EHPs' recombination greatly [26–29]. However, most of the studies investigated the TiO_2 nanoparticle-based photocatalytic performance. Previous investigations indicate that one-dimensional TiO_2 nanofiber structure could bring extra superiorities over those nanoparticle counterparts. Those beneficial factors contributed by one-dimensional structure include better crystallinity, low density of surface defects and direct transfer channel enabling the acceleration of electron transport and more efficient inhibition of interfacial recombination rate. In addition, effective contact between photocatalysts and pollutants was endowed by large surface area. Moreover, a more convenient separation and recovery was enabled by collecting the accumulated nanofibers forming a unique mascroscopic mat [2].

It has been demonstrated that combining one-dimensional TiO_2 nanomaterials with GQDs provides a credible solution tackling the problem of organic pollutants. In one of our previous publications [2], one-dimensional TiO_2 nanofibers matrix has been

successfully prepared by means of electrospinning, which provides a good substrate for the successive combination with GQDs. The GQDs were obtained from graphene sheets with an average size about 2–3 μm by hydrothermal stripping. A novel structure of GQDs-decorated one-dimensional TiO_2 electrospun nanofibers was successfully synthesized. The composite exhibited a one-dimensional structure with diameters around 200 nm. In addition, its photocatalytic degradation properties for methylene blue (MB) were examined. The as-prepared TiO_2/GQDs were tested to display a superior photocatalytic performance with comparison to pure TiO_2 nanofibers.

Experimental

Materials

Tetrabutyl titanate (TBT, 5593-70-4 (CAS No.), $\geq$ 98.0% (purity)), polyacrylonitrile (PAN, 25014-41-9, M_w = 150,000), methylene blue (MB, 61-73-4, 95%), polyvinylpyrrolidone (PVP, 9003-39-8, M_w = 1,300,000), dimethylformamide (DMF, 68-12-2, $\geq$ 99.5%), acetic acid (64-19-7, $\geq$ 99.8%), graphene (1034343-98-0, 97%) and ammonium hydroxide (1336-21-6, 25–28%) were commercial products, and deionized water was self-made.

Synthesis of TiO_2 hollow nanofibers (TiO_2 HNFs)

Electrospinning technique and subsequent calcination were used to synthesize TiO_2 HNFs. A weight of 2.5 g TBT was added drop-wise to 2.5 g of acetic acid with continuous stirring to prepare electrospinning solution. Another solution containing 2 g of PVP, 1 g of PAN and 20 g of DMF was mixed with stirring. Then, this mixture was mixed with the above TBT solution. The electrospinning parameters are as follows: The flow rate of precursor solution in the syringe was set to 0.05 mm/min, output voltage is 15 kV, distance from needle to receiver collector is 20 cm, temperature is kept constant as 35 °C, and humidity is 50%. The specimens thus obtained were subsequently pre-oxidized by a furnace set at 200 °C for a duration 2 h and calcined at 500 °C for a duration of 3 h.

Preparation of GQDs

A typical preparation of GQDs was carried out by hydrothermal method. Ten milligrams of graphene powders was dissolved with 50 ml deionized water. The solution was ultrasonicated for 10 min to make sure of the homogeneity and then transferred to a hydrothermal kettle. Aqueous solution of GQDs was kept at the temperature of 200 °C for a duration of 12 h. The prepared GQDs were cooled down to room temperature for subsequent preparation of composite.

Preparation of TiO_2 HNFs-GQDs composite

Composite nanofibers were prepared by hydrothermal method. TiO_2 HNFs and GQDs were added into a teflon stainless-steel reaction kettle, and then aqueous solution of mixture was kept in the temperature condition of 180 °C for 12 h. Solution of composite nanofiber thus obtained was dried to form powder for the subsequent test. When the GQDs content ratio within the composite for photocatalytic degradation test, which is calculated by (the respective amount of graphene powder)/(the amount of TiO_2 HNFs-GQDs composite) is 5%, 8%, 10%, 12.5% and 15% of the composite, they are denoted as TGs5, TGs8, TGs10, TGs12.5 and TGs15, respectively. The GQDs ratio in the composite of the specimens made for characterization tests (except photocatalytic degradation) is 10%, as marked in the respective figure captions.

Characterization

SEM and TEM were utilized to analyze the morphology. XRD was performed to investigate the crystallographic structure. PL properties were characterized by Fluorescence spectrophotometer. XPS was measured utilizing an Al-K-Alpha source gun. Ultraviolet–visible light absorption spectra (UV–Vis) were measured utilizing a spectrophotometer to determine the concentration of the pollutant MB at certain irradiation time intervals.

Photocatalytic activity measurements

Photocatalytic activity of synthesized specimens was characterized by its degradation toward MB by light irradiation (290–800 nm). For the photocatalytic

degradation experiments, 20 mg of TiO$_2$ HNFs-GQDs composite was added in 100 ml of a 5 mg/l MB dye solution. Under magnetic stirring, the mixed suspension was irradiated under 500-W xenon lamp. In addition, a control experiment with 20 mg of pure TiO$_2$ HNFs was also carried out to monitor photocatalytic activity. Prior to light condition, the suspension was placed in dark condition with constant stirring for 30 min to reach a MB's adsorption equilibrium onto the photocatalysts. In the process of light irradiation, at pre-defined time interval, 5 ml of suspension was taken out and centrifuged for 5 min at an 8000 r/min spinning speed before the UV–Vis characterization ($\lambda = 664$ nm). According to the Lambert–Beer law, the absorption changes (C_t/C_0 ratio) of the MB dye during the photodegradation are proportional to A_t/A_0 ratio of maximum absorption peak.

Result and discussion

Figure 1 shows schematically the preparation process of TiO$_2$ HNFs, GQDs and subsequent synthesis of composites. In this reaction protocol, the one-dimensional mesoporous structure of electrospun TiO$_2$ HNFs was obtained through electrospinning the mixed precursor solution containing TBT, PAN and PVP and subsequent calcination. Thus, a tubular TiO$_2$ nanofiber structure with mesoporous characteristics (SEM and BET characterization in [2]) serves as a substrate for GQDs. The as-prepared aqueous solution of GQDs was directly mixed with TiO$_2$ HNFs to act as the hydrothermal precursor materials. The open mesoporous structure and large surface area produced more active sites, which can facilitate the interaction between GQDs and mesoporous TiO$_2$ [2, 30]. It is reported that the hydrothermal "sintering" conditions could enable GQDs to be deposited stably onto the surface of TiO$_2$, without free-standing GQDs in the water [28]. GQDs can be well dispersed with both the surface and internal structure of TiO$_2$ HNFs, thus forming a firm composite in the hydrothermal synthesis.

GQDs with a size less than 10 nm and a uniform shape and size distribution were successfully prepared as in Fig. 2. The prepared sample was elliptically shaped with size centered at 4 ± 2 nm, but a small portion of the sample was oversized. The reason for this phenomenon is related to their respective preparation methods: In the hydrothermal reaction process, the peeling effect under high temperature and high pressure is difficult to control. In addition, the raw material is relatively large (micron order); therefore, it is difficult to peel all the raw materials into products of uniform size. It can be observed that the GQDs obtained by this method show exclusively graphene lattice spacing ($d = 0.216$ nm), indicating that hydrothermal process is an appropriate recipe to manufacture GQDs possessing uniform size distribution. PL spectra in Fig. 2d exhibit that GQDs display an excitation-dependent PL behavior with a remarkable up-conversion feature at excitations from 650 to 800 nm [30, 31]. As the wavelength of excitation was displaced through the region of 650–800 nm, the up-converted emission peaks was observed to display a red shift from 480 to 580 nm with intensity increasing. The property of converting the excitation light in the infrared wavelength range into a shorter

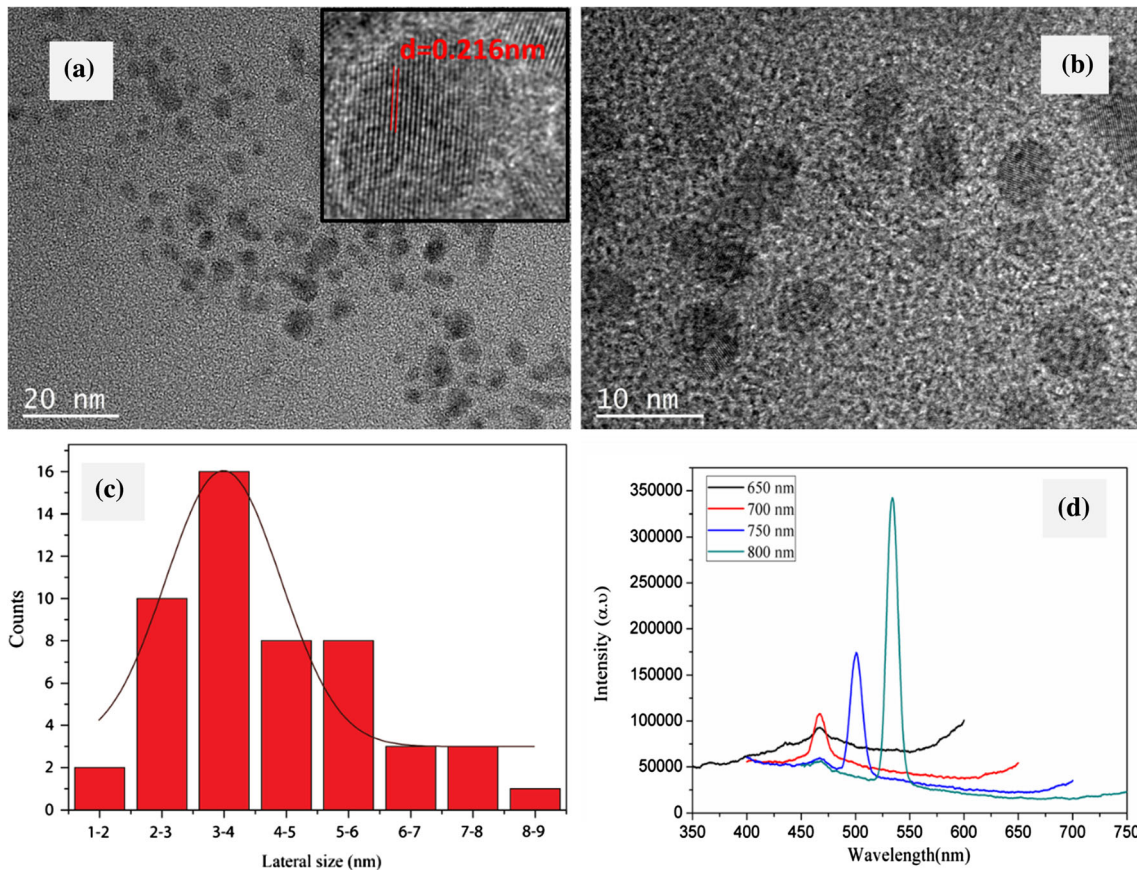**Figure 1** Scheme of synthesizing process of the composites.
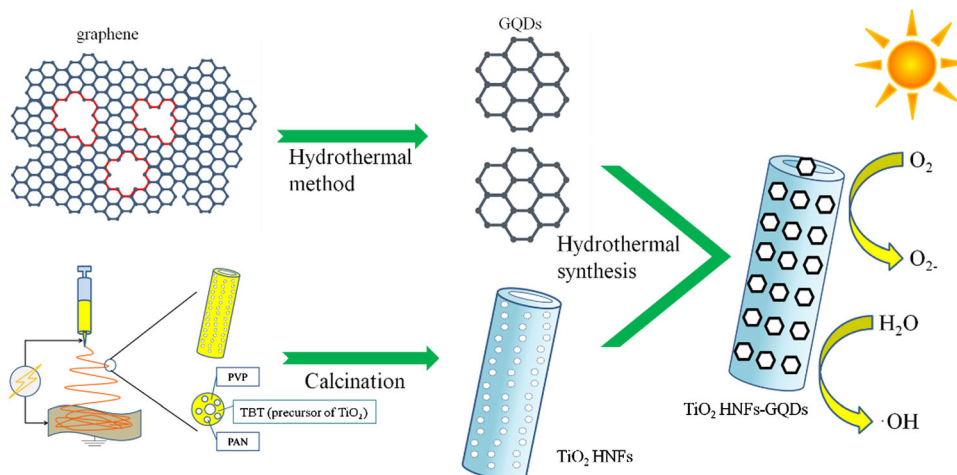
Figure 2 **a**, **b** TEM images of GQDs, inset of **a** showing lattice spacing; **c** statistical chart of GQDs size distribution; the black line indicates the Gauss fit of size distribution of GQDs. **d** PL spectra of GQDs.

wavelength of emitted light enables more sunlight to be utilized in photocatalytic reaction, which can improve the catalytic performance significantly. The reason for this phenomenon is that there are many defect state energy levels in GQDs, and the low-energy excitation can only trigger the electron transition from the π orbital to excited state. Subsequently, electrons in the π^* orbital can transit to the lower-leveled σ orbital, leading to a shorter-wavelength light emission [30, 31].

As presented in Fig. 3a TiO$_2$ HNFs have a high ratio of length to diameter and a diameter about 200–300 nm. It is apparent that the nanofibers have a large number of surface wrinkles and internal passages that can be used as decorative parts for GQDs. Such TiO$_2$ HNFs have less resistance to charge flow because there is less grain binding between them compared to TiO$_2$ nanoparticles. Figure 3b shows that the prepared TiO$_2$ HNFs have a distance of 0.352 nm between adjacent lattice stripes,

corresponding to the anatase TiO$_2$ (101) plane, which has an ultra-high photocatalytic activity [32, 33].

In Fig. 3c, d, after the decoration of GQDs, TiO$_2$ HNFs still retain the one-dimensional nanofiber morphology. GQDs have no significant effect on the macroscopic morphology of TiO$_2$ HNFs. Figure 3e characterizes the internal pores of TiO$_2$ composite nanofibers. The interface between GQDs and TiO$_2$ is presented in Fig. 3f. High-resolution TEM (HRTEM) image shows that GQDs are surrounded by both anatase and rutile phase. At the same time, EDX elemental mapping was performed on TiO$_2$ HNFs-GQDs composite to study the spatial distribution of each element. The results show that Ti, C and O are uniformly distributed throughout the nanofibers, as shown in Fig. 3g–j. Among them, Ti and O are constituent elements of TiO$_2$, and C is a constituent element of GQDs.

The crystallographic structure of TiO$_2$ HNFs, GQDs and composite was investigated by means of XRD measurements (Fig. 4). TiO$_2$ HNFs and its

Figure 3 a SEM and **b** TEM images of TiO$_2$ HNFs; **c, d** SEM images of TiO$_2$-GQDs (10%); **e, f** TEM images of TiO$_2$-GQDs (10%); **g** overlay images of Ti, C and O elements by EDX elemental mapping of TiO$_2$-GQDs (10%); **h**–**j** EDX elemental mapping of Ti, C and O elements, respectively.
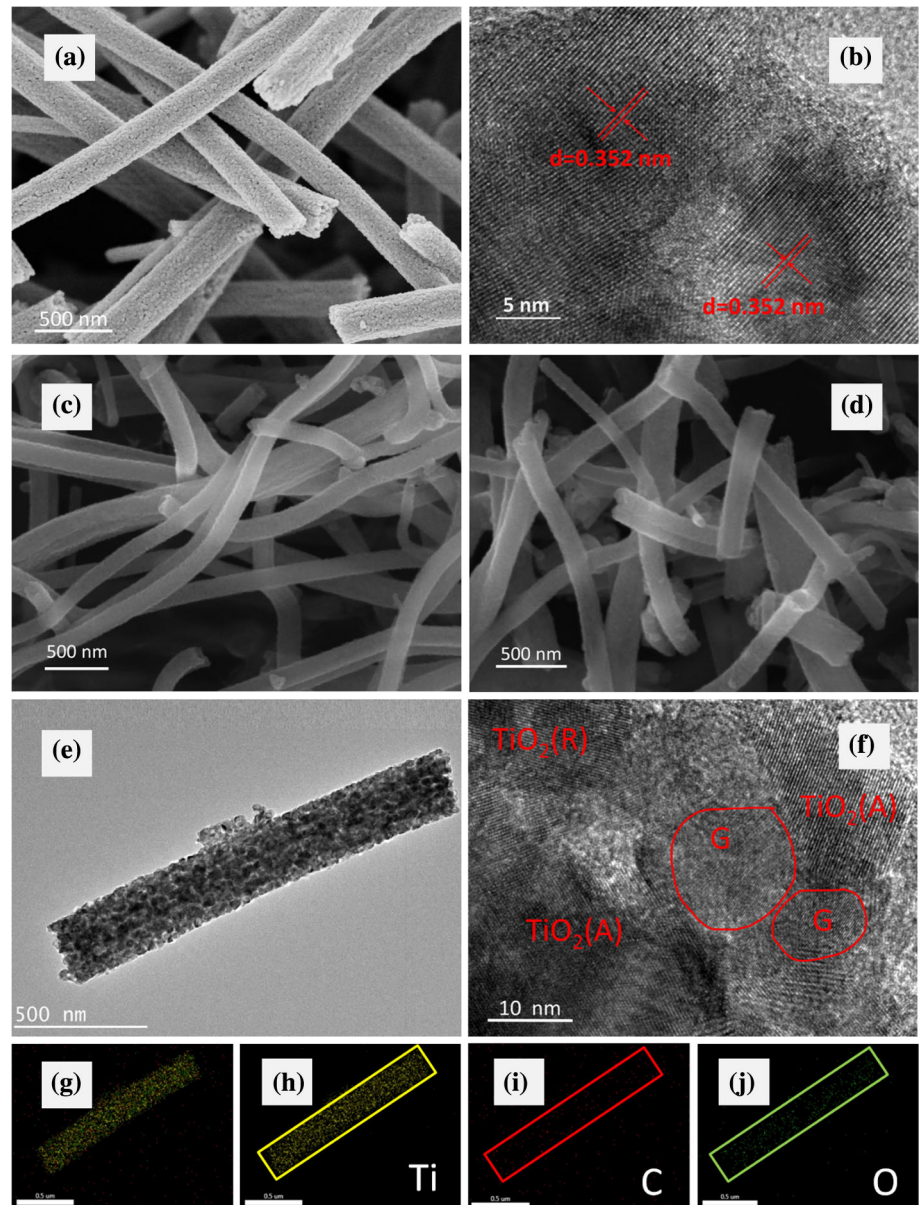
composite exhibit distinct peaks contributed by TiO$_2$, with diffraction peaks ascribed to (101), (105), (200), (211), (004), (215) and (204) crystal planes of anatase phase and peaks ascribed to (110), (220), (301) and (112) crystal planes of rutile phase, which are in good agreement with JCPDS data (PDF#21-1272 and PDF#21-1276, respectively) and consistent with our TEM results. This typical anatase crystal indicates a higher photocatalytic activity. The diffraction peaks attributed to carbon species did not appear in the composites with GQDs decoration, which was owing to low content and lower diffraction intensity of the carbon element. In addition, graphene has a

characteristic peak at 24.5° in the neighborhood of peaks at 25.3° ascribed to anatase (101) planes with much higher intensity; thus, they cannot be easily observed.

From the perspective of crystallite size, the size of TiO$_2$ HNFs-GQDs increased from 16.38 to 17.67 nm, compared to the specimen without GQDs. This was explained by GQDs' fusion through the pores of TiO$_2$ HNFs in hydrothermal process.

As in Fig. 5a, the XPS survey spectra display the appearance of Ti, O and C elements by peaks at binding energies of Ti 2p (459.76 eV), O1s (531.0 eV), and C1s (285.22 eV), respectively. Especially the
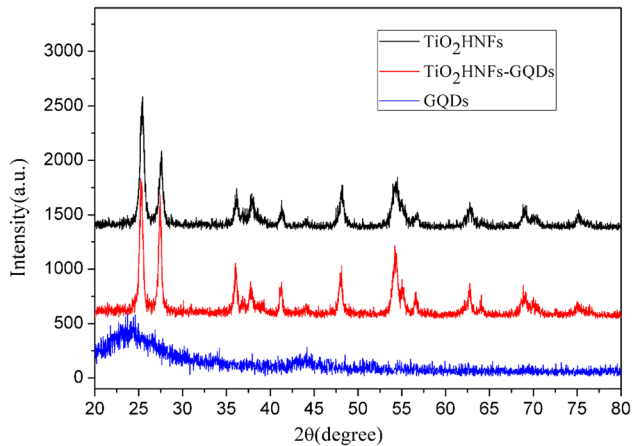
Figure 4 XRD spectra of GQDs, TiO$_2$ HNFs and the composite TiO$_2$ HNFs-GQDs (10%).

C1s peak at 285.22 eV of TiO$_2$ HNFs-GQDs is significantly more intense than that of pure TiO$_2$ HNFs, which could be explained by addition of GQDs into TiO$_2$ HNFs, which is consistent with TEM analysis. The main C 1s peak from deconvolution at 284.8 eV is because of carbon hybridized in $\underline{sp}^2$ form (C=C bond). At higher binding energy tails, two peaks at 285.2 and 286.5 eV are observed, which could be ascribed to hybridized carbon in sp^3 form and the species with C–O bond. The peak at 288.3 eV is characteristics of Ti–O–C structure, indicating the C atoms' doping into TiO$_2$ lattice during preparation [32], the bond of which made composites connect more closely. As shown in Fig. 5c, the O 1s signal can be deconvoluted into three peaks at 530.8 (Ti–O–Ti bond), 532.4 (Ti–OH bond), and 533.5 eV (C–OH bond), respectively [30, 34]. It is noticeable to indicate Ti 2p3/2 has a higher binding energy value of 459.6 eV, compared to that of pure TiO$_2$ HNFs (458.88 eV), which can be explained by C doping among the composite, thus inducing the upper shift of binding energy in Ti 2p3/2.

The UV–Vis diffuse reflection spectra were performed for analyzing optical absorption property in specimens. TiO$_2$ HNFs and TiO$_2$ HNFs-GQDs show absorption edges at about 380 nm and 460 nm,
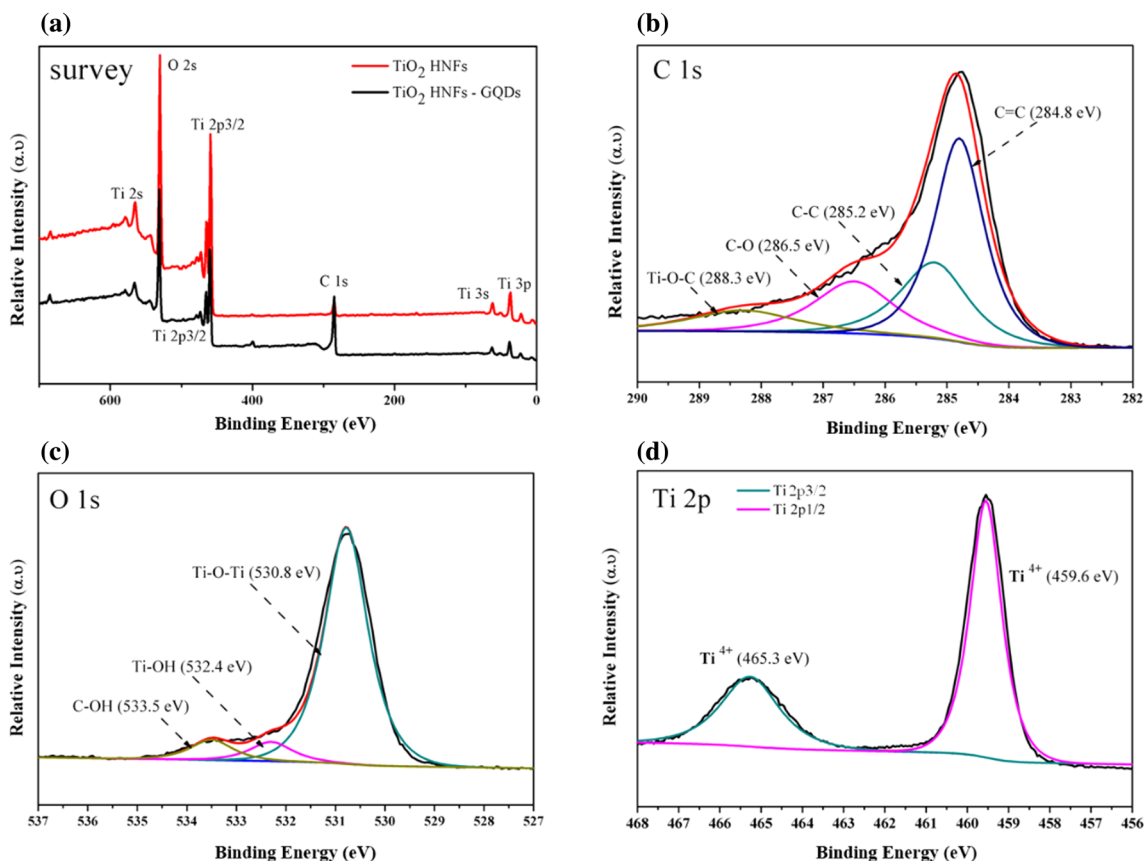

Figure 5 XPS analysis of **a** the survey spectra of TiO$_2$ HNFs (black line), TiO$_2$ HNFs-GQDs (10%, red line), **b** C1s, **c** O1s and **d** Ti2p spectra of the composite (TiO$_2$ HNFs-GQDs, 10%).

respectively (Fig. 6a). A red shift in absorption band edge of about 80 nm to higher wavelength has been observed in TiO_2 HNFs-GQDs with respect to the pure TiO_2 HNFs, indicating the composite photocatalyst had a narrower band gap with the graphene introduction [35]. The Kubelka–Munk equation was utilized to calculate the band gap of the materials, and the results exhibited that the band gap for TiO_2 HNFs is 3.24 eV, whereas it is 2.98 eV for TiO_2 HNFs-GQDs. It can be seen that the band gap has been narrowed down by the introduction of GQDs. This phenomenon can be attributed to the incorporation of auxiliary electron acceptor (GQDs), which could absorb visible light [36, 37] and thus formed Ti–O–C bonding facilitates charge transfer [38, 39].

To further clarify the role that GQDs can play in the composite photocatalytic system, PL characterization was performed to investigate their function in prohibition of charge carriers' recombination. In principle, a typical photocatalytic scheme involves the excitation, bulk diffusion and surface transfer of EHPs. While the separated charge carriers participated in organic molecule degradation, most photoinduced EHPs easily recombine at the trapping sites, and subsequent photons release accordingly, resulting in PL [40]. The PL peak corresponds to the direct recombination of EHPs at oxygen defects, impurities and surface defects [27]. For both samples, the PL peaked around 480 nm (Fig. 6b). However, the peak intensity of the TiO_2 HNFs-GQDs composite is noticeably reduced from the respective peak height of TiO_2 HNFs because the recombination of photogenerated EHPs was inhibited by GQDs due to their excellent charge carrier transfer ability [34].

Figure 7 shows the photocatalytic degradation efficiency of TiO_2 HNFs, TiO_2 HNFs-GQDs toward MB solution under light irradiation (290–800 nm). The composite displayed a significantly more efficient degradation performance. After 50 min of catalytic reaction (dark reaction for 30 min, photoreaction for 20 min), TiO_2 HNFs discolored MB by 46%, and the reduction of MB in the solution by means of TGs5, TGs8 and TGs10 was 48%, 84% and 99%, respectively. It is obvious that the composite with 10% GQDs content has the best catalytic properties. The above results indicate that a certain mass fraction of GQDs has a great effect on improving the catalytic removing ability of TiO_2 composite photocatalyst. However, the degradation properties of the composite photocatalyst do not monotonically increase with increasing GQDs content. It can be clearly seen that TGs12.5 and TGs15 have shown a further decrease in degradation ratio (91% and 75%, respectively). This might be explained by the involvement with GQDs, that to some extent covers the main photoactive sites [41]. It needs to be pointed out that the degradation cannot primarily be due to the dark adsorption, because as observed in Fig. 7, the photodegradation continuously occurs during the whole procedure after light irradiation is switched on. On the other hand, the excessive decoration of GQDs on TiO_2 would lead to a deterioration of the degradation performance, which is a distinctive feature of photocatalytic degradation.

The excellent degradation properties of TiO_2/GQDs composites photocatalyst are mainly attributed to three aspects: Firstly, the electrons and holes induced by ultraviolet and visible-light irradiation
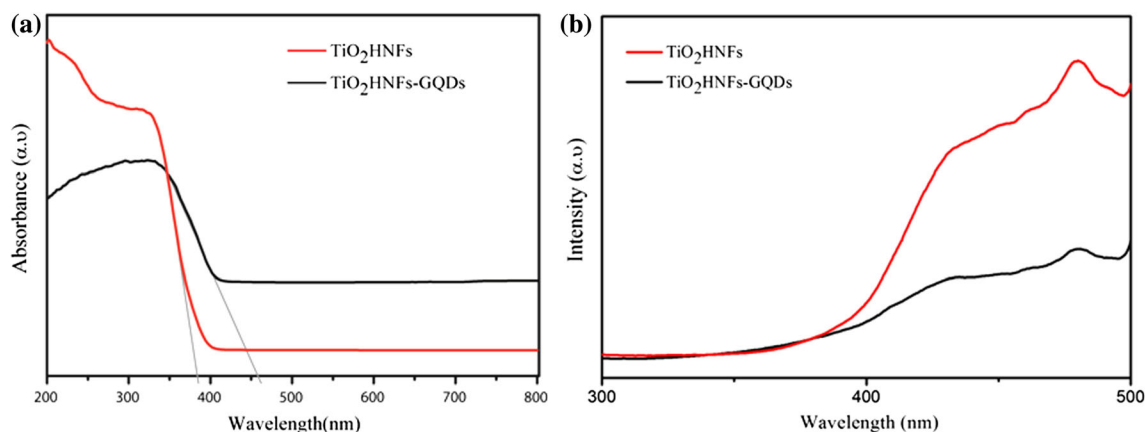

Figure 6 **a** UV–Vis spectra of **a** TiO_2 HNFs and TiO_2 HNFs-GQDs (10%); **b** PL emission spectra of TiO_2 HNFs and TiO_2 HNFs-GQDs (10%) at 252 nm excitation wavelength.
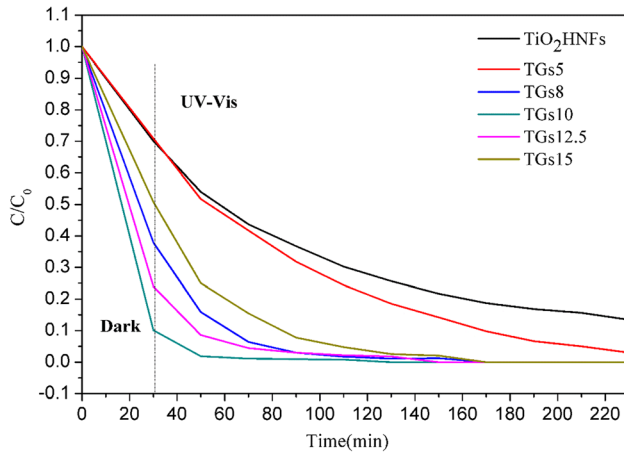
Figure 7 Photodegradation ratio to MB for TiO$_2$ HNFs, TiO$_2$ HNFs-GQDs.

band where is in close contact with GQDs which can act as an electron reservoir to trap photogenerated electrons, so as to promote efficient EHPs' transfer to separated sites, resulting in better photocatalytic properties for dye degradation [44, 45]. Due to the unique features of their up-conversion in PL process, GQDs can work as effective converters of energy. The GQDs can transfer long wavelength irradiation light ($\lambda > 650$ nm) into the shorter-wavelength emission light to be utilized efficiently by TiO$_2$ HNFs-GQDs composite. One additional key factor affecting the improved photocatalytic performance is that TiO$_2$'s bonding with the OH groups of graphene's surface in the form of Ti–O–C chemical correlation, which extends absorption band edge [46].

are effectively separated by GQDs, which significantly improves the degradation process. The excellent electronic conductivity of GQDs enables them to be ideal electron transport paths through interconnected composites, which prohibits the adverse recombination between photoinduced charges. Secondly, the photoluminescence effect of GQDs expands the photoresponse range of composite photocatalysts. Lastly, GQDs retain the graphene geographic configuration possessing a high specific surface area for effective contact between pollutants and the composite [42, 43]. Therefore, the TiO$_2$-GQDs material's photocatalytic activity was significantly improved.

The speculated schematic diagram of TiO$_2$ HNFs-GQDs composite photocatalyst under illumination is shown in Fig. 8. Upon irradiation, electrons are excited and transit from valence band to conduction

Conclusion

A facile synthesis procedure has been demonstrated for the manufacture of TiO$_2$ HNFs-GQDs composite nanofibers by electrospinning combined with hydrothermal method. GQDs with several nanometer sizes presented were composited with TiO$_2$ HNFs, retaining a one-dimensional structure. The unique property of up-conversion in emission light of GQDs enabled more efficient light utilization for successive photodegradation. PL characterization of composites proved that GQDs inhibited the recombination rate of charge carriers and prolonged the existence of photogenerated holes, leading to improved photodegradation.

The photocatalytic activities characterization results show that TiO$_2$ HNFs-GQDs composites had better degradation properties due to ultrafast electron
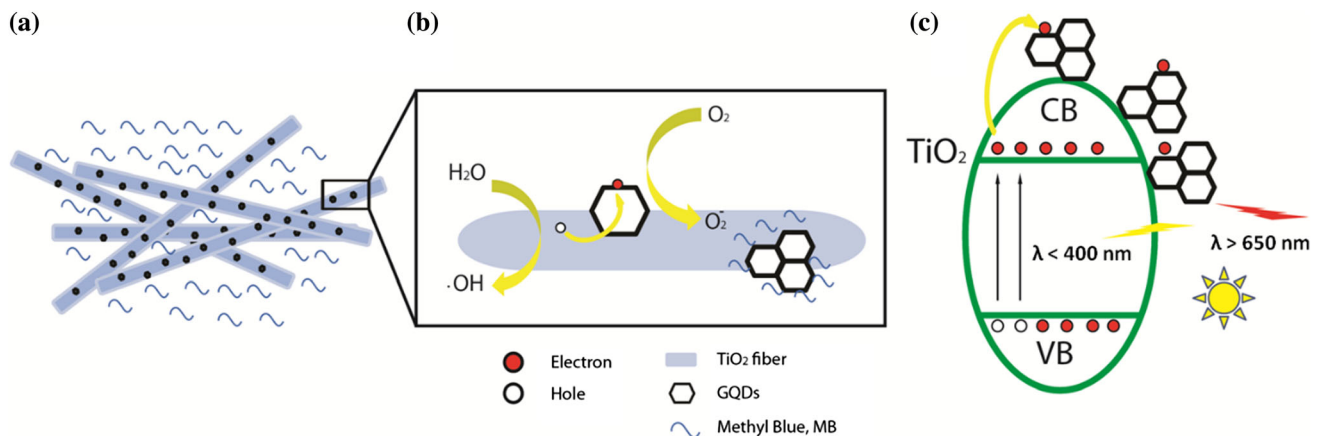

Figure 8 The schematic diagram of degradation process for GQDs-decorated TiO$_2$ composite structure.

transport rate and low photogenerated carrier recombination compared with pure TiO_2 catalyst. The degradation properties do not monotonically increase with GQDs content, and it was observed that a further decrease occurred when GQDs was excessive. To sum up, electron transfer, photogenerated carriers' recombination and light adsorption properties are important factors that affect the photocatalytic properties.

Acknowledgements

References

[1] Liu R, Hayden HL, Suter H, Hu H, Lam SK, He J, Mele PM, Chen D (2017) The effect of temperature and moisture on the source of N_2O and contributions from ammonia oxidizers in an agricultural soil. Biol Fertil Soils 53:141–152. https://doi.org/10.1007/s00374-016-1167-8

[2] Zhao P, Huo P, Han X, Liu B (2019) Enhanced photodegradation activity of electrospun porous TiO_2 fibers. Funct Mater Lett 12:1941002. https://doi.org/10.1142/S1793604719410029

[3] Huo P, Zhao P, Wang Y, Liu B, Dong M (2018) An effective utilization of solar energy: enhanced photodegradation efficiency of TiO_2/graphene-based composite. Energies 11:630. https://doi.org/10.3390/3n11030630

[4] Moon G, Kim D, Kim H, Bokare AD, Choi W (2014) Platinum-like behavior of reduced graphene oxide as a cocatalyst on TiO_2 for the efficient photocatalytic oxidation of arsenite. Environ Sci Technol Lett 1:185–190. https://doi.org/10.1021/ez5000012

[5] Zhang H, Guo L, Wang D, Zhao L, Wan B (2015) Light-induced efficient molecular oxygen activation on a Cu(II)-grafted TiO_2/graphene photocatalyst for phenol degradation. ACS Appl Mater Interfaces 7:1816–1823. https://doi.org/10.1021/am507483q

[6] Xian J, Li D, Chen J, Li X, He M, Shao Y, Yu L, Fang J (2014) TiO_2 nanotube array-graphene-CdS quantum dots composite film in Z-scheme with enhanced photoactivity and photostability. ACS Appl Mater Interfaces 6:13157–13166. https://doi.org/10.1021/am5029999

[7] Liu H, Wang X, Wu D (2017) Fabrication of graphene/TiO_2/paraffin composite phase change materials for enhancement of solar energy efficiency in photocatalysis and latent heat storage. ACS Sustain Chem Eng 5:4906–4915. https://doi.org/10.1021/acssuschemeng.7b00321

[8] Kwon H, Marques Mota F, Chung K, Jang YJ, Hyun JK, Lee J, Kim DH (2018) Enhancing solar light-driven photocatalytic activity of mesoporous carbon–TiO_2 hybrid films via upconversion coupling. ACS Sustain Chem Eng 6:1310–1317. https://doi.org/10.1021/acssuschemeng.7b03658

[9] Lannoy A, Bleta R, Machut-Binkowski C, Addad A, Monflier E, Ponchel A (2017) Cyclodextrin-directed synthesis of gold-modified TiO_2 materials and evaluation of their photocatalytic activity in the removal of a pesticide from water: effect of porosity and particle size. ACS Sustain Chem Eng 5:3623–3630. https://doi.org/10.1021/acssuschemeng.6b03059

[10] Perera SD, Mariano RG, Vu K, Nour N, Seitz O, Chabal Y, Balkus KJ (2012) Hydrothermal synthesis of graphene-TiO_2 nanotube composites with enhanced photocatalytic activity. ACS Catal 2:949–956. https://doi.org/10.1021/cs200621c

[11] Kamegawa T, Yamahana D, Yamashita H (2010) Graphene coating of TiO_2 nanoparticles loaded on mesoporous silica for enhancement of photocatalytic activity. J Phys Chem C 14:15049–15053. https://doi.org/10.1021/jp105526d

[12] Pan X, Yang M, Tang Z, Xu Y (2014) Noncovalently functionalized graphene-directed synthesis of ultralarge graphene-based TiO_2 nanosheet composites: tunable morphology and photocatalytic applications. J Phys Chem C 118:27325–27335. https://doi.org/10.1021/jp507173a

[13] Zhang P, Hou X, Liu L, Mi J, Dong M (2015) Two-dimensional π-conjugated metal bis(dithiolene) complex nanosheets as selective catalysts for oxygen reduction reaction. J Phys Chem C 119:28028–28037. https://doi.org/10.1021/acs.jpcc.5b09148

[14] Sun D, Zhang Y, Liu Y, Wang Z, Chen X, Meng Z, Kang S, Zheng Y, Cui L, Chen M, Dong M, Hu B (2020) In-situ homodispersely immobilization of Ag@AgCl on chloridized g-C_3N_4 nanosheets as an ultrastable plasmonic photocatalyst. Chem Eng J 384:123259. https://doi.org/10.1016/j.cej.2019.123259

[15] Kuznetsov VN, Serpone N (2009) On the origin of the spectral bands in the visible absorption spectra of visible-light-active TiO_2 specimens analysis and assignments. J Phys Chem C 113:15110–15123. https://doi.org/10.1021/jp901034t

[16] Choi J, Park H, Hoffmann MR (2010) Effects of single metal-ion doping on the visible-light photoreactivity of TiO_2. J Phys Chem C 114:783–792. https://doi.org/10.1021/jp908088x

[17] Pan H, Zhang YW, Shenoy VB, Gao H (2011) Effects of H-, N-, and (H, N)-doping on the photocatalytic activity of TiO_2.

J Phys Chem C 115:12224–12231. https://doi.org/10.1021/jp202385q

[18] Valero JM, Obregón S, Colón G (2014) Active site considerations on the photocatalytic H_2 evolution performance of Cu-doped TiO_2 obtained by different doping methods. ACS Catal 4:3320–3329. https://doi.org/10.1021/cs500865y

[19] Zhou H, Pan J, Ding L, Tang Y, Ding J, Guo Q, Fan T, Zhang D (2014) Biomass-derived hierarchical porous CdS/M/TiO_2 (M = Au, Ag, Pt, Pd) ternary heterojunctions for photocatalytic hydrogen evolution. Int J Hydrog Energy 39:16293–16301. https://doi.org/10.1016/j.ijhydene.2014.08.032

[20] Ferrari AC, Meyer JC, Scardaci V, Casiraghi C, Lazzeri M, Mauri F, Piscanec S, Jiang D, Novoselov KS, Roth S, Geim AK (2006) Raman spectrum of graphene and graphene layers. Phys Rev Lett 97:187401. https://doi.org/10.1103/PhysRevLett.97.187401

[21] Pang X, Zhang Y, Liu C, Huang Y, Wang Y, Pan J, Wei Q, Du B (2016) Enhanced photoelectrochemical cytosensing of fibroblast-like synoviocyte cells based on visible light-activated ox-GQDs and carboxylated g-C_3N_4 sensitized TiO_2 nanorods. J Mater Chem B 4:4612–4619. https://doi.org/10.1039/C6TB00295A

[22] Shen K, Xue X, Wang X, Hu X, Tian H, Zheng W (2017) One-step synthesis of band-tunable N, S co-doped commercial TiO_2/graphene quantum dots composites with enhanced photocatalytic activity. RSC Adv 7:23319–23327. https://doi.org/10.1039/C7RA01856H

[23] Salam Z, Vijayakumar E, Subramania A, Sivasankar N, Mallick S (2015) Graphene quantum dots decorated electrospun TiO_2 nanofibers as an effective photoanode for dye sensitized solar cells. Sol Energy Mater Sol Cells 143:250–259. https://doi.org/10.1016/j.solmat.2015.07.001

[24] Shen J, Zhu Y, Yang X, Li C (2012) Graphene quantum dots: emergent nanolights for bioimaging, sensors, catalysis and photovoltaic devices. Chem Commun 48:3686–3699. https://doi.org/10.1039/C2CC00110A

[25] Zhang B, Gao H, Li X (2014) Synthesis and optical properties of nitrogen and sulfur co-doped graphene quantum dots. New J Chem 38:4615–4621. https://doi.org/10.1039/c4nj00965g

[26] Qu A, Xie H, Xu X, Zhang Y, Wen S, Cui Y (2016) High quantum yield graphene quantum dots decorated TiO_2 nanotubes for enhancing photocatalytic activity. Appl Surf Sci 375:230–241. https://doi.org/10.1016/j.apsusc.2016.03.077

[27] Gupta BK, Kedawat G, Agrawal Y, Kumar P, Dwivedi J, Dhawan SK (2015) A novel strategy to enhance ultraviolet light driven photocatalysis from graphene quantum dots infilled TiO_2 nanotube arrays. RSC Adv 5:10623–10631. https://doi.org/10.1039/c4ra14039g

[28] Pan D, Jiao J, Li Z, Guo Y, Feng C, Liu Y, Wang L, Wu M (2015) Efficient separation of electron–hole pairs in graphene quantum dots by TiO_2 Heterojunctions for dye degradation. ACS Sustain Chem Eng 3:2405–2413. https://doi.org/10.1021/acssuschemeng.5b00771

[29] Safardoust-Hojaghan H, Salavati-Niasari M (2017) Degradation of methylene blue as a pollutant with N-doped graphene quantum dot/titanium dioxide nanocomposite. J Clean Prod 148:31–36. https://doi.org/10.1016/j.jclepro.2017.01.169

[30] Miao R, Luo Z, Zhong W, Chen S, Jiang T, Dutta B, Nasr Y, Zhang Y, Suib SL (2016) Mesoporous TiO_2 modified with carbon quantum dots as a high-performance visible light photocatalyst. Appl Catal B 189:26–38. https://doi.org/10.1016/j.apcatb.2016.01.070

[31] Shen J, Zhu Y, Chen C, Yang X, Li C (2011) Facile preparation and upconversion luminescence of graphene quantum dots. Chem Commun 47:2580–2582. https://doi.org/10.1039/c0cc04812g

[32] Setvin M, Shi X, Hulva J, Simschitz T, Parkinson GS, Schmid M, Di Valentin C, Selloni A, Diebold U (2017) Methanol on anatase TiO_2 (101): mechanistic insights into photocatalysis. ACS Catal 7:7081–7091. https://doi.org/10.1021/acscatal.7b02003

[33] Setvin M, Hulva J, Wang H, Simschitz T, Schmid M, Parkinson GS, Di Valentin C, Selloni A, Diebold U (2017) Formaldehyde adsorption on the anatase TiO_2(101) surface: experimental and theoretical investigation. J Phys Chem C 121:8914–8922. https://doi.org/10.1021/acs.jpcc.7b01434

[34] Pu S, Zhu R, Ma H, Deng D, Pei X, Qi F, Chu W (2017) Facile in-situ design strategy to disperse TiO_2 nanoparticles on graphene for the enhanced photocatalytic degradation of rhodamine 6G. Appl Catal B 218:208–219. https://doi.org/10.1016/j.apcatb.2017.06.039

[35] Zhang L, Zhang J, Jiu H, Ni C, Zhang X, Xu M (2015) Graphene-based hollow TiO_2 composites with enhanced photocatalytic activity for removal of pollutants. J Phys Chem Solids 86:82–89. https://doi.org/10.1016/j.jpcs.2015.06.018

[36] Yang J, Zhang X, Li B, Liu H, Sun P, Wang C, Wang L, Liu Y (2014) Photocatalytic activities of heterostructured TiO_2-graphene porous microspheres prepared by ultrasonic spray pyrolysis. J Alloys Compd 584:180–184. https://doi.org/10.1016/j.jallcom.2013.08.203

[37] Lettmann C, Hildenbrand K, Kisch H, Macyk W, Maier WF (2001) Visible light photodegradation of 4-chlorophenol with a coke-containing titanium dioxide photocatalyst. Appl Catal B 32:215–227. https://doi.org/10.1016/S0926-3373(01)00141-2

[38] Sakthivel S, Kisch H (2003) Daylight photocatalysis by carbon-modified titanium dioxide. Angew Chem Int Ed 42:4908–4911. https://doi.org/10.1002/anie.200351577

[39] Ren W, Ai Z, Jia F, Zhang L, Fan X, Zou Z (2007) Low temperature preparation and visible light photocatalytic activity of mesoporous carbon-doped crystalline TiO_2. Appl Catal B 69:138–144. https://doi.org/10.1016/j.apcatb.2006.06.015

[40] Gu L, Wang J, Cheng H, Zhao Y, Liu L, Han X (2013) One-step preparation of graphene-supported anatase TiO_2 with exposed 001 facets and mechanism of enhanced photocatalytic properties. ACS Appl Mater Interfaces 5:3085–3093. https://doi.org/10.1021/am303274t

[41] Wang X, Wang J, Dong X, Zhang F, Ma L, Fei X, Zhang X, Ma H (2016) Synthesis and catalytic performance of hierarchical TiO_2 hollow sphere/reduced graphene oxide hybrid nanostructures. J Alloys Compd 656:181–188. https://doi.org/10.1016/j.jallcom.2015.09.241

[42] Liu S, Liu C, Wang W, Cheng B, Yu J (2012) Unique photocatalytic oxidation reactivity and selectivity of TiO_2–graphene nanocomposites. Nanoscale 4:3193–3200. https://doi.org/10.1039/c2nr30427a

[43] Zhang Z, Xiao F, Guo Y, Wang S, Liu Y (2013) One-pot self-assembled three-dimensional TiO_2-graphene hydrogel with improved adsorption capacities and photocatalytic and electrochemical activities. ACS Appl Mater Interfaces 5:2227–2233. https://doi.org/10.1021/am303299r

[44] Wang P, Wang J, Ming T, Wang X, Yu H, Yu J, Wang Y, Lei M (2013) Dye-sensitization-induced visible-light reduction of graphene oxide for the enhanced TiO_2 photocatalytic performance. ACS Appl Mater Interfaces 5:2924–2929. https://doi.org/10.1021/am4008566

[45] Byeon JH, Kim Y (2013) Gas-phase self-assembly of highly ordered titania@graphene nanoflakes for enhancement in photocatalytic activity. ACS Appl Mater Interfaces 5:3959–3966. https://doi.org/10.1021/am400765z

[46] Wang W, Wang D, Qu W, Lu L, Xu A (2012) Large ultrathin anatase TiO_2 nanosheets with exposed 001 facets on graphene for enhanced visible light photocatalytic activity. J Phys Chem C 116:19893–19901. https://doi.org/10.1021/jp306498b